

AD A 056428

# LEVEL II



SABOT DESIGN FOR A 105MM APFSDS KINETIC ENERGY PROJECTILE,

11 JUN 1978

10 WILLIAM H. DRYSDALE, DR.  
RICHARD D. KIRKENDALL, MR.  
LOUISE D. KOKINAKIS, MS.

US ARMY BALLISTIC RESEARCH LABORATORY  
ABERDEEN PROVING GROUND, MD 21005

12 15 P.

DDC  
REC'D  
JUL 10 1978  
REGISTRY

AD No. 1  
JDC FILE COPY

Increased projectile muzzle velocity and extended range can be achieved with a given gun system through the use of a sub-caliber projectile with a discarding sabot. This improvement occurs because the bore area on which the gun pressure acts may be greatly increased with only a relatively modest increase in total projectile weight, and the small diameter flight body has less aerodynamic drag. Obviously, to obtain the optimum performance improvement, the sabot mass must be kept as low as possible within the constraints set by the structural requirements of the sabots.

Foremost of these requirements is that the sabot must ensure the in-bore operation of the projectile, i.e., it must be able to seal the gun tube against the hot propellant gas. Then, especially for long rod kinetic energy penetrators, the sabot must provide enough support to prevent the subprojectile from being permanently deformed in an undesirable manner during in-bore travel. Also, the sabot must constrain the subprojectile during in-bore travel and then discard in such a manner as to impart small initial yaw and yaw rate to the subprojectile during launch. These parameters are related to target dispersion and should be reduced as much as possible. Finally, the sabot will generally provide the means for assembly of the full round. Hence, such matters as fin encroachment into the cartridge case and location of crimping grooves so that the assembled round can withstand rough handling should be considered.

In the discussion to follow, we will assume that the penetrator diameter, length, and material, fins and nosecone (in

DISTRIBUTION STATEMENT A

Approved for public release;  
Distribution Unlimited

50 750  
78 06 12 001



\*DRYSDALE, KIRKENDALL, KOKINAKIS

smaller restoring moments experienced during in-bore operation allow lighter weight sabots.

Locating the rotating band near the center of the projectile required a change in the long ramp-back sabot design of the 60mm AAAC projectile. The rear ramp was shortened by using a compound taper. To maintain the favorable uniform shear load transfer which is possible under a taper, a front ramp was added ahead of the centered rotating band. This configuration is the basis of the BRL Double-Ramp Sabot.

Calculation of Taper Profile. As mentioned previously, one of the primary reasons for adapting a ramp-back sabot is the self-sealing nature of this configuration. The propellant gas operating on the tapered surfaces creates very high compressive hoop and radial stresses. These stresses are higher than the gas pressure, so there is no tendency for pressure to leak into narrow splits between sabot petals, forcing them apart.

It has been realized for many years that a long ramp-back sabot configuration might enable subprojectiles to be launched without driving grooves. The high compressive radial stress at the sabot/subprojectile interface under a rear taper, in combination with a reasonable coefficient of friction, could allow the entire shear load to be transferred from the sabot by friction alone (1). A very recent study has attempted to determine the minimum weight taper profile which would transfer a given shear load from sabot to subprojectile without exceeding a specified friction coefficient (2). The minimum weight shape did not give a uniform shear transfer along the interface. However, the use of some very severe restrictions (e.g., a rigid subprojectile) make the practical application of this work doubtful.

The methodology of calculating the shape of a long rear taper for a cylindrical penetrator is based on elementary free-body stress analysis, combined with well known solutions of closely related problems. The basic procedure was developed by Dr. Bruce P. Burns of BRL during the 60mm AAAC Technology Program. The taper profiles are designed to provide a uniform shear transfer along the interface at the maximum chamber pressure condition.

The external base pressure and the projectile acceleration may be found from interior ballistic considerations based on an approximate projectile weight. The initial stress in the penetrator at the edge of the sabot is determined from the unsupported length of rod, weight of fins or nosecone, and the acceleration. In the derivations to follow, a subscript  $s$  will refer to the sabot and

subscript p will refer to the penetrator or subprojectile.

The free bodies shown in Figure 1 are formed from the projectile by planes perpendicular to the axis. The segment is thin enough that the outer contour may be replaced by a straight line, forming a truncated conical segment. Squares and higher powers of  $\Delta Z$  will be ignored compared to one. In addition, the slope of the contour will be assumed to be small. It is further assumed that the axial stress in each component is constant over the cross section, or, alternately that only average axial stresses are considered. The shear  $\tau$  is to be constant in the axial coordinate and may be assigned any desired value. The object is to determine  $R(Z)$ , the shape of the contour, which will accomplish this.

Summing the forces defined in Figure 1a acting on the sabot in the axial direction, with consideration of the mentioned assumptions, gives

$$(1) \quad (P_0 + \sigma_{Zs}) \frac{d\phi}{dZ} + \left( -\frac{d\sigma_{Zs}}{dZ} - \rho_s \ddot{Z} \right) \phi = 2\tau R_p$$

where the unknown is

$$\phi = R^2 - R_p^2 ; \quad \phi = \phi_0 \text{ at } Z = 0.$$

To be able to solve this relation for  $\phi$ , the axial sabot stress must be known.

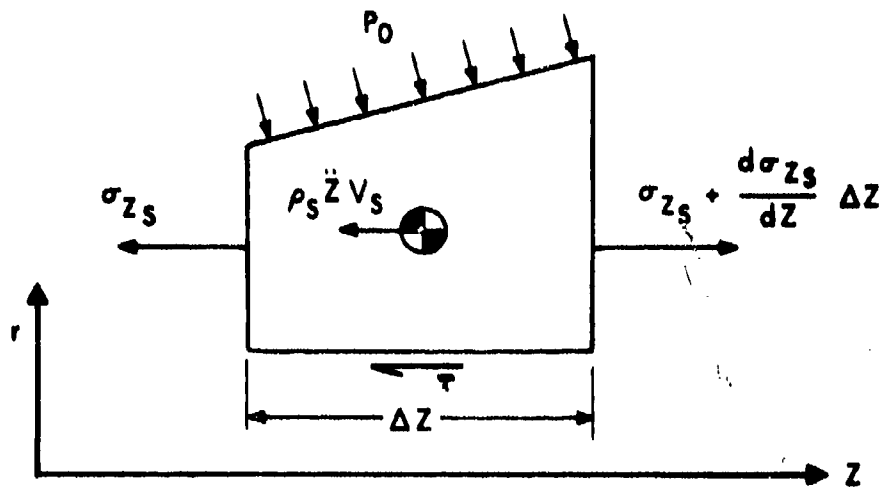
Along the interface between sabot and penetrator, the axial displacement is the same in both components (no slip condition). Hence the axial strain is equal across the interface. Utilizing Hooke's Law for elastic materials, the sabot axial stress may be found as

$$(2) \quad \sigma_{Zs} = \frac{E_s}{E_p} [\sigma_{Zp} - \nu_p(\sigma_r - \sigma_\theta)_p] + \nu_s(\sigma_r + \sigma_\theta)_s$$

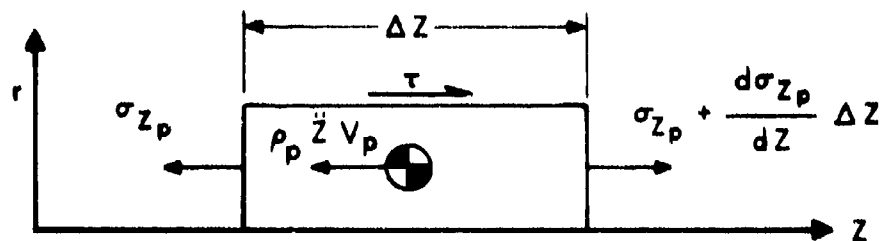
Summing forces acting on the penetrator, as shown in Figure 1b gives, after integrating

$$(3) \quad \sigma_{Zp} = \left( \rho_p \ddot{Z} - \frac{2\tau}{R_p} \right) Z + \sigma_0$$

It remains to determine  $(\sigma_r + \sigma_\theta)$  for the sabot and penetrator in terms of the known pressure and material properties. For the



a. Sabot Stress System



b. Penetrator Stress System

Figure 1. Free Body Diagram for Sabot and Penetrator Stresses

configuration under consideration, this would be a very difficult problem. The difficulty may be eliminated by appealing to the smallness of the taper ratio and the principle of superposition of stresses in order to consider only stresses in the  $r - \theta$  plane. Then the stress state may be approximated by the Lamé solution for elastic circular cylindrical bodies of dissimilar materials acted on by external pressure. The pressure at the interface in the Lamé solution is determined by matching the radial displacements there as

$$P_i = 2R^2 P_o [(R^2 + R_p^2) + \nu_s (R^2 - R_p^2) + \frac{E_s}{E_p} (1 - \nu_p)(R^2 - R_p^2)]^{-1}$$

If this relation were used in the differential equation for  $R$ , the result would be a highly nonlinear expression due to the appearance of  $R^2$  in the coefficients. To sidestep this difficulty, the limits of  $P_i$  as  $R$  approaches both  $R_p$  and large possible values are determined, and the numerical average used as the constant value of  $P_i$  for all values of  $R$ . This is

$$(4) \quad 2P_i = [3 + \nu_s + \frac{E_s}{E_p} (1 - \nu_p)] P_o [1 + \nu_s \frac{E_s}{E_p} (1 - \nu_p)]^{-1}$$

If equations (2), (3) and the Lamé solution for  $(\sigma_r + \sigma_\theta)$ , using equation (4) for interface pressure are substituted into the differential equation (1), the solution may be found by integration as

$$(5) \quad \phi = [\phi_o - \frac{2\tau}{\alpha} R_p] \left[ \frac{\Sigma_o}{\Sigma_o + (\rho_p Z - \frac{2\tau}{R_p})Z} \right]^B + \frac{2\tau}{\alpha} R_p$$

where  $\Sigma_o = \sigma_o + 2\nu_p P_i + \frac{E_p}{E_s} (1 - 2\nu_s) P_o$

$$\alpha = \frac{E_s}{E_p} (\rho_p Z - \frac{2\tau}{R_p}) - \rho_s Z$$

$$B = 1 - \frac{E_p}{E_s} \frac{\rho_s Z}{(\rho_p Z - \frac{2\tau}{R_p})}$$

$$\phi_o = R^2(0) - R_p^2$$

\*DRYSDALE, KIRKENDALL, KOKINAKIS

Up to the present the derivation has implicitly considered the rear taper. However, the same analysis applies to the forward taper. Since there is no propellant gas operating, the pressures are zero. In using the formula for ramp profile, the taper begins at the origin of the Z axis. Thus the slope of both front and rear tapers is positive. Care must be exercised with the sign of other quantities; however, especially the shear and acceleration, depending on the configuration under investigation.

The taper profile calculated from the formula is nonlinear. Within the accuracy of the analysis and when only the lower portion of the ramp is to be used in a compound taper, the actual R curve may often be replaced by a linear interpolation for ease of machining.

The formula as derived could certainly be improved. Ignoring the axial stresses while applying the Lamé solution is inconsistent at least. Axisymmetric stress solutions exist which improve the estimate of  $\sigma_{\theta}$  being constant over the penetrator cross-section. Use of axial stress values corrected for nonuniformity at the interface improve the taper predictions. However, it would be inappropriate to develop the approximate analysis too far. Its purpose is to give an initial estimate of a taper profile which permits uniform shear transfer at the sabot/penetrator interface. The predictions of the formula should be checked and improved if necessary by use of an axisymmetric, elastic, finite element code. Only by this procedure may the approximate analysis be justified.

The concept of the double-ramp as opposed to the more conventional sabot configuration may be illustrated by finite element analysis of two examples. In Figure 2 is seen a saddle-back sabot, with the pressure acting on the rear face of the sabot. To illustrate the shear load transfer qualities, no acceleration will be imposed on this example. The parameters used in the calculations are shown in Table I.

A dot is used in Figure 2 to locate each element of the sabot that has a tensile hoop stress. A segmented sabot cannot support hoop tension, so the seams must open in these regions. The areas of hoop tension form a path completely through the sabot, which would open to gas flow. Also shown is the shear stress variation at the interface. The result is very nonuniform, with a peak of nearly 344.75 MPa at the ends, falling to low values in the center. This type of variation is conducive to domino failures, with shear grooves failing sequentially along the interface.

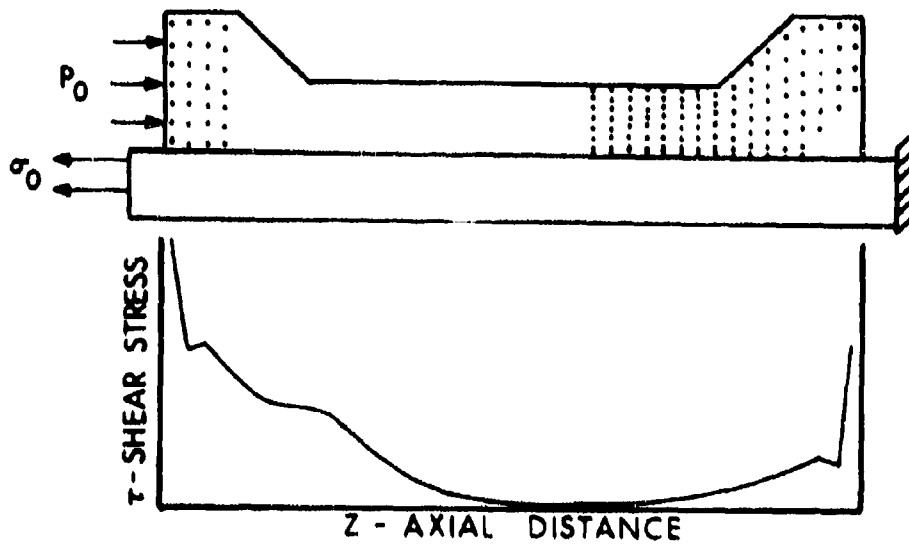


Figure 2. Conventional Saddle-Back Sabot Configuration

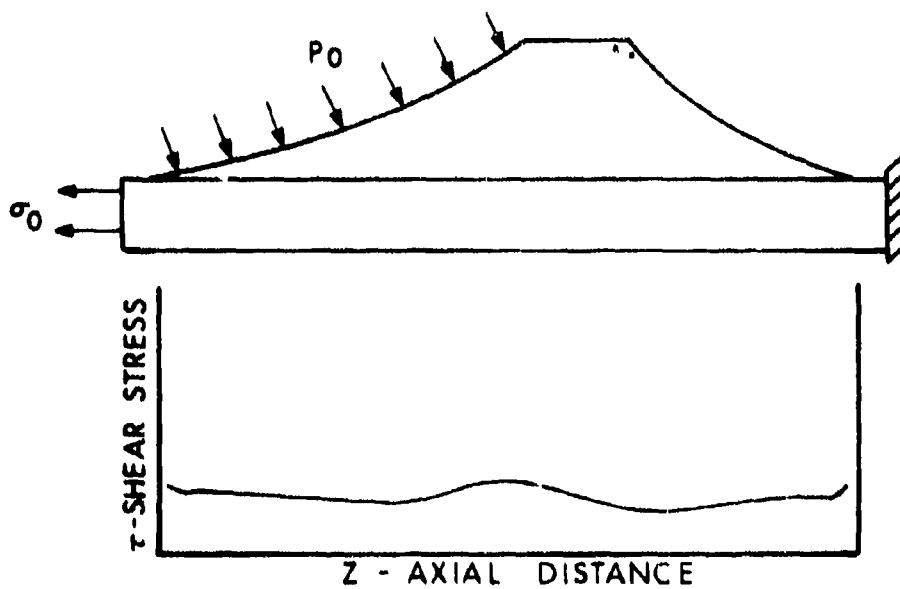


Figure 3. BRL Double-Ramp Sabot Configuration

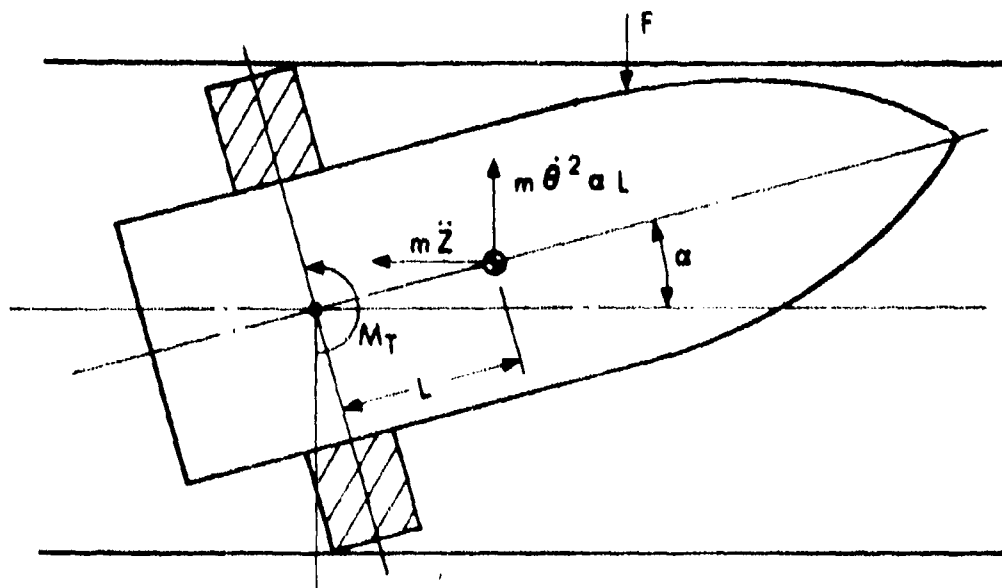
Table I. Properties of Sabot and Penetrator

$E_p = 275,800 \text{ MPa}$	$V_p = V_s = .3$
$E_s = 68,950 \text{ MPa}$	$R_p = .0254 \text{ m}$
$Z = 0$	$R_{\text{Bore}} = .0762 \text{ m}$
$P_o = 172.38 \text{ MPa}$	Length of Sabot = .254 m
$\sigma_o = 689.5 \text{ MPa}$	

The same material and loading parameters were used to calculate the stresses in a double-ramp sabot, shown in Figure 3. The desired shear stress at the interface was 68.95 MPa. Only two elements near the forward taper had hoop tension. The shear stress at the interface is relatively uniform, differing by less than 20.69 MPa from the projected value.

Both numerical examples were calculated with the SAAS II axisymmetric, elastic finite element code. They clearly present the advantages to be expected from a double-ramp sabot configuration with respect to self-sealing of gas pressure and uniform transfer of load from sabot to subprojectile.

In-Bore Rigid Body Dynamics. The lack of in-bore stability of a projectile has important consequences for its overall performance. It has been realized for at least 100 years that locating the rotating band at the projectile center of gravity improves in-bore stability (3). Reasons for this conclusion may be demonstrated using rigid body dynamics. Figure 4 is a conceptual diagram of a conventional projectile during its in-bore travel. It is assumed that the rotating band acts as a centering device and that, therefore, transverse yawing motion must be about an axis through the band. The center of gravity is located at a distance L ahead of the pivot axis. Clearances and eccentricities of parts cause the axis of the projectile to deviate from the centerline of the tube during in-bore travel and move the center of gravity away from the axis of the tube. The setback force, due to the acceleration of the projectile, will be a vector parallel to the gun axis, which will create an overturning moment  $M_t$  about the pivot. If the gun tube is rifled, the



$$M_T = m\ddot{z}aL + m\dot{\theta}^2 aL^2$$

Figure 4. In-Bore Rigid Body Dynamic Configuration

\*DRYSDALE, KIRKENDALL, KOKINAKIS

centrifugal force due to the spin of the eccentric projectile will also produce a moment. The magnitude of the total moment is

$$M_T = MZ\ddot{\alpha}L + M\dot{\theta}^2 \alpha L^2$$

and it is unstable in the sense that any yaw angle, no matter how small, generates a moment which operates to increase yaw. This unstable growth of yaw angle increases until the front bourrelet impacts the tube wall, after which the projectile will travel the remaining distance cocked at the maximum possible yaw attitude. The overturning moment is countered by the moment produced about the pivot by the force  $F$  applied to the forward bourrelet. This force is reduced by the adaptation of a longer wheelbase or distance to the front bore rider. Even so, this transverse force may be substantial. The structure supporting the front bore rider must suffer the weight penalty necessary to adequately resist the load.

As the length  $L$  approaches zero, the configuration of a centered rotating band appears. For this case, any small disturbance will not result in the unstable growth of yaw, because the moment arm is zero. This situation would normally be called neutrally stable, since as presented, there is no moment which would tend to eliminate an initial yaw. However, in a much more detailed dynamic analysis performed by L. H. Thomas (4), it was shown that, for the case  $L = 0$ , the gyroscopic moments due to spin would act to realign the projectile and tube axes.

To ensure that the rotating band was centered over the position of the c.g., use was made of two computer codes for calculating the rigid body properties of objects. The first is a locally derived code which finds the properties (weight, c.g., moments of inertia) of axisymmetric shapes or segments by numerical integration. The second code, known as MOMENTS II (5), can combine several basic shapes or defined shapes (such as are determined from the first code) into a total body. As any design changes affecting the taper angles, fin weight, etc. are made, the rotating band may be relocated over the center of gravity in an iterative manner. In this way the in-bore stability of the projectile is maintained.

Other Details. There is a multitude of other details that must be considered by the designer which will only be alluded to in this section. Since the double-ramp sabot is a centered configuration, the length of penetrator extending fore and aft of the sabot must be determined. When the penetrator length is known, this calculation also determines the minimum sabot length.

\*DRYSDALE, KIRKENDALL, KOKINAKIS

In order to determine the allowable stress level in a structural component in a triaxial state of stress, the effective or equivalent stress of plasticity theory is used. It is well known that this parameter correlates with plastic yield much better than maximum normal stress. The effective stress level in the free fore and aft length of the rod depends only on the acceleration forces acting on the subprojectile, since a uniform hydrostatic pressure has no effect on effective stress level. The unsupported lengths are chosen to give the desired stress immediately aft and forward of the sabot.

The above value of unsupported length must be checked for stability problems. One such check is for column buckling. Expressions for determining the critical length of a fixed-free column in a uniform acceleration field may be found in many handbooks. Likewise, the problem of the whirling of a shaft with an end mass (such as fins) will have some critical length which must not be exceeded for each value of projectile spin allowed.

Under the rear taper the ratio of interface radial stress to shear stress can be made nearly constant and less than some maximum allowable value of friction coefficient. In this area, no grooves or other load transfer devices are necessary (1). In the other portions of the sabot/penetrator interface, the resultant shear load must be carried by threads or grooves. The number of grooves per inch is determined by equating the product of allowable bearing stress and bearing area with the shear force per inch of interface to be transmitted. To obtain the highest possible groove strength in the dissimilar sabot and penetrator materials, equal shear area grooves should not be used. The areas of the root of a tooth in the sabot and rod is ratioed inversely to the ultimate strengths of the two materials so that both components may carry the same load.

After the initial design calculations have been performed, the candidate design and all further iterations should be thoroughly investigated with a reliable stress analysis code. Ideally a fully three-dimensional dynamic analysis simulating the interior ballistic process should be performed. We have settled for an axisymmetric, quasi-static analysis at peak pressure and acceleration.

One of the primary results of an analysis as described is a map of effective stress in the projectile. In the ATTGI program, this effective stress was required to be below the plastic yield stress of the respective material. It may be appreciated that this is an overly conservative requirement, since plastic flow does not of itself mean failure in a single use component. The adaption of a more sophisticated

\*DRYSDALE, KIRKENDALL, KOKINAKIS

failure criteria would be a very fruitful modification of the current design procedure.

Test Results and Discussion. Two separate models of the BRL double-ramp sabot were designed as part of the ATTGI program. A high-pressure version capable of operating at maximum chamber pressures of 730.87 MPa was initially tested, but not pursued. A low-pressure version operating at standard 105mm tank gun pressures was also designed and tested more extensively.

A sketch of the low-pressure BRL double-ramp projectile is shown in Figure 5. It has been successfully fired during high temperature tests to a peak chamber pressure of 572.29 MPa. Three of the early versions of this projectile suffered rotating band failures, which are believed to have been caused by excessive interference due to tolerance buildup. Even though the sabots suffered severe gas wash due to loss of the band, there was no gas leakage between sabot petals or at the sabot/penetrator interface. No rotating band failures have occurred since this band was redimensioned (28 rounds fired).

Included within the ATTGI program was the development of an advanced conventional saddle-back sabot. Effectively the same subprojectile was used in both this sabot and the BRL double-ramp, so comparisons of performance are easily made. For the full in-bore 105mm projectile, the BRL double-ramp weighed slightly over .4536 Kg less than the conventional sabot. This translates into a muzzle velocity increase of 57.3 m/s for the subprojectile. The initial yaw of the free flight subprojectile was measured from yaw cards approximately 40 m from the muzzle. These measurements showed nearly the same average value of yaw for the BRL double-ramp and the conventional saddle-back sabot. Likewise, the target dispersion at 1,000 meters, based on very small samples, was essentially equal.

It had been anticipated that the centered rotating band of the BRL double-ramp sabot would result in substantial reductions in initial yaw and, consequently, target dispersion, over the conventional configuration. Instead the values of these parameters are nearly equal for the two sabots. Development of the double-ramp, by the lengthening of the wheelbase and/or the use of full projectile spin, will continue in the future and should reveal the advantages in reduced yaw and target dispersion of which the stable in-bore configuration is capable.

The BRL double-ramp configuration has been demonstrated to be a very effective sabot for launching kinetic energy penetrators. However, the concepts involved are applicable whenever it is desired to obtain higher velocity or increased range by use of a sabot.

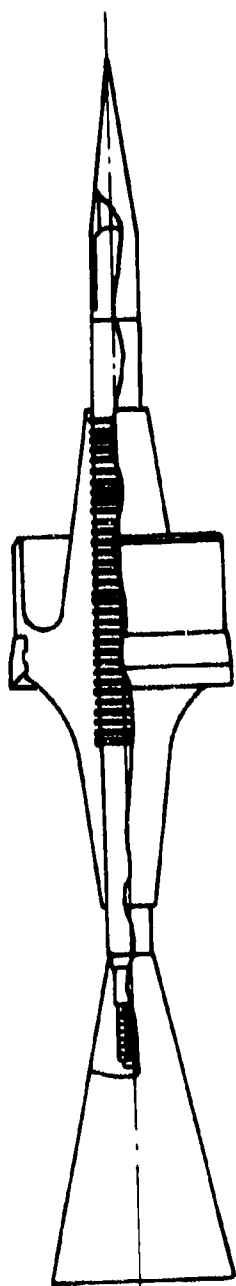


Figure 5. BRL Double-Ramp Sabot as Tested in 105mm ATTCI Program

\*DRYSDALE, KIRKENDALL, KOKINAKIS

References

- (1) "Development of a Special Type Small Arms Cartridge (Sabot Supported)" (U) (Confidential Report); Aircraft Armaments, Inc., Report No. ER-1414, July 1958, AD 300912.
- (2) Chun, Y. W. and Haug, E. J., "Two Dimensional Shape Optimal Design," Technical Report No. 38, Division of Materials Engineering, Univ. of Iowa, January 1978.
- (3) Breger, Captain M. P., "Position and Form of Bands for Projectiles," *Memoires Militaires et Scientifiques*, publies par le Department de la Marine, translated by Lt. C. C. Morrison, Ordnance Dept., U.S.A., in "Notes on the Construction of Ordnance, No. 27," Washington, D. C., June 1884.
- (4) Thomas, L. H., "The Motion of the Axis of a Spinning Shell Inside the Bore of a Gun," Report No. 544, USA Ballistic Research Laboratories, Aberdeen Proving Ground, MD, May 1945, AD PB22102.
- (5) Lacher, E. B., "Moments II - A Computer Program to Calculate Moments and Products of Inertia of Asymmetric Objects," Technical Report No. 4945, Picatinny Arsenal, NJ, May 1976.